energies

Article

Cogging Force Reduction and Profile Smoothening Methods for a Slot-Spaced Permanent Magnet Linear Alternator

Chin-Hsiang Cheng [1,*] and Surender Dhanasekaran [2]

[1] Department of Aeronautics and Astronautics, National Cheng Kung University, Tainan City 70101, Taiwan
[2] International Doctoral Degree Program on Energy Engineering, National Cheng Kung University, Tainan City 70101, Taiwan; surenderdhanasekaran@gmail.com
* Correspondence: chcheng@mail.ncku.edu.tw; Tel.: +886-6-2757575 (ext. 63627)

Abstract: A Permanent Magnet Linear Alternator (PMLA) works seamlessly with a Free Piston Stirling Engine (FPSE) to convert short-stroke and high-frequency linear motion to electric power. Cogging force is an unavoidable opposition force acting on the translator, limiting the linear motion from the driving force, which shortens the lifespan of the machine, causing oscillatory power output and increased maintenance costs. This research focuses on the methods to reduce the cogging force acting on the translator of a slot-spaced PMLA by making geometrical changes to the structure of the machine. The profile of the cogging force is made to be in line with the displacement profile of the translator to avoid unnecessary vibrations and damaging the piston of the FPSE. The changes made also influence the induced voltage. Bringing a balance between reduced voltage and cogging force with minor geometrical changes and a sinusoidal cogging force profile is the outcome of this work.

Keywords: cogging force; notching; permanent magnet linear alternator; PMLSM

check for updates

Citation: Cheng, C.-H.; Dhanasekaran, S. Cogging Force Reduction and Profile Smoothening Methods for a Slot-Spaced Permanent Magnet Linear Alternator. *Energies* **2023**, *16*, 5827. https://doi.org/10.3390/en16155827

Academic Editors: Luca Del Zotto and Luca Cioccolanti

Received: 14 July 2023
Revised: 31 July 2023
Accepted: 4 August 2023
Published: 6 August 2023

1. Introduction

The usage of fossil fuels for energy production has damaged the global climate significantly over decades. The limitation of global warming levels within 1.5–2.0 °C is imminent as per the Paris Agreement. The risk of losing the Greenland ice sheets and flooding of the Amazon rainforests is inevitable without these capping levels [1]. Continued usage of fossil fuels will result in the flooding of global rivers and elevated levels of thermal ranges in the marine ecosystem [2,3]. To replace the usage of fossil fuels with renewable and clean energy in power production, it would take an eight-fold change to shift completely by 2050 [4]. The nearest prediction of global clean energy production in 2024 is 33%. Rigorous developments and continuous advancements in green energy production are an imminent requirement to fight climate change.

Wave Energy Converters (WEC) have been gaining popularity in the recent past and they have a huge potential in filling the space to replace conventional energy production methods [5]. FPSEs are an alternative source of clean energy production, and they have been gaining popularity in the recent past. The ability to generate power from waste heat recovery systems as low as 300 °C has been possible and developments in the advancements have been rising continuously [6]. To eliminate mechanical losses and make use of the linear drive motion directly, WECs and FPSEs use linear over rotary alternators. WECs have a high stroke length and low frequency, and FPSEs have, vice versa, a high frequency and low stroke length. However, due to the versatility and its advantages of having high operational velocity, precise movement and control, prolonged life, and efficiency, PMLAs have grown in favor over rotary counterparts for power generation in WECs, thermoacoustic engines, Hybrid Electric Vehicles (HEV), FPSEs, and suspension systems of HEVs [7–12].

Cogging force is a parasitic force caused by the magnetic attraction between the stator teeth and the permanent magnets mounted on the translator. Due to the attraction, the permanent magnets intend to stay aligned with the stator teeth and thus act as an opposing force to the driving force that produces power [13]. The cogging force is a crucial factor to consider in the design of a PMLA because it affects the performance and efficiency of the machine. It causes significant losses in the machine, resulting in reduced efficiency and increased heat generation.

In a linear alternator, the cogging force can cause significant mechanical stress on the moving parts, leading to increased wear and tear and potential damage to the machine. It also causes the moving parts to vibrate, which can reduce the stability and accuracy of the machine, and potentially lead to mechanical failure over time. Additionally, the cogging force can also affect the power output of the machine. If the cogging force is too high, it can make it difficult for the moving part to follow the desired motion, reducing the overall power output of the PMLA. On the other hand, if the cogging force is too low, it can result in reduced efficiency, as more energy is lost as heat instead of being converted into useful electric power.

Therefore, it is important to consider the cogging force in the design process of a PMLA, as it can have a significant impact on the performance and efficiency of the machine. This requires the careful selection of the materials and dimensions of the magnetic circuit, as well as careful control of the current flowing in the coils, to ensure optimal performance and reliability. Hence, the profile of the cogging force is expected to be the same as the displacement profile of the translator, and cogging force levels are expected to be as minimal as possible without affecting the power output from the machine [14]. The phase angle difference between the displacement and cogging force is expected to be negligible. This study is aimed at reducing the cogging force of the slot-spaced PMLA model by not reducing the induced voltage by a significant margin and making the cogging force profile match the displacement profile of the translator.

2. Slot-Spaced PMLA Model

2.1. Structure

The structure and parametric analysis of this slot-spaced PMLA model is backed by our previous research [15,16]. A tubular topology is preferred over a flat-type PMLA [8]. The Quasi-Halbach (QH) model is used for creating strong and weak sections to the magnet to have a high-power density machine with effective utilization of space on the translator [17]. Slot space in between the teeth of the stator is introduced to shave away excess material and create a lighter stator to increase the overall power density. Figure 1 shows a complete illustration of a cut-section view of the machine.

The copper coil is a toroidal wound and is arranged in an asymmetrical pattern. There are 960 turns in each coil. The internal resistance of the copper coil is 5 Ω. The stator and translator shaft have 35CS300H, and the magnet concerning the material choice has N48H. The overall dimensions of the machine are mentioned in Table 1.

Table 1. Geometrical parameters of the original PMLA.

Parameters	Dimensions (mm)
Stator Stack Length, S_l	110
Back Iron Thickness, B_t	2.5
Stator Outer Diameter, S_o	100
Slot height, S_h	23.5
Slot Width, S_w	10
Tooth slot gap, T_s	5
Tooth thickness, S_t	5
Tooth slot thickness, S_s	2.5
Shaft Stack Length, H_l	110
Coil Outer Diameter, C_o	95
Coil Inner Diameter, C_i	48
Magnet Outer Diameter, M_d	46
Radial Magnet thickness, M_r	15
Axial Magnet thickness, M_a	7.5
Air gap, g	1
Shaft Outer Diameter, H_d	25
Shaft Inner Diameter, H_i	15

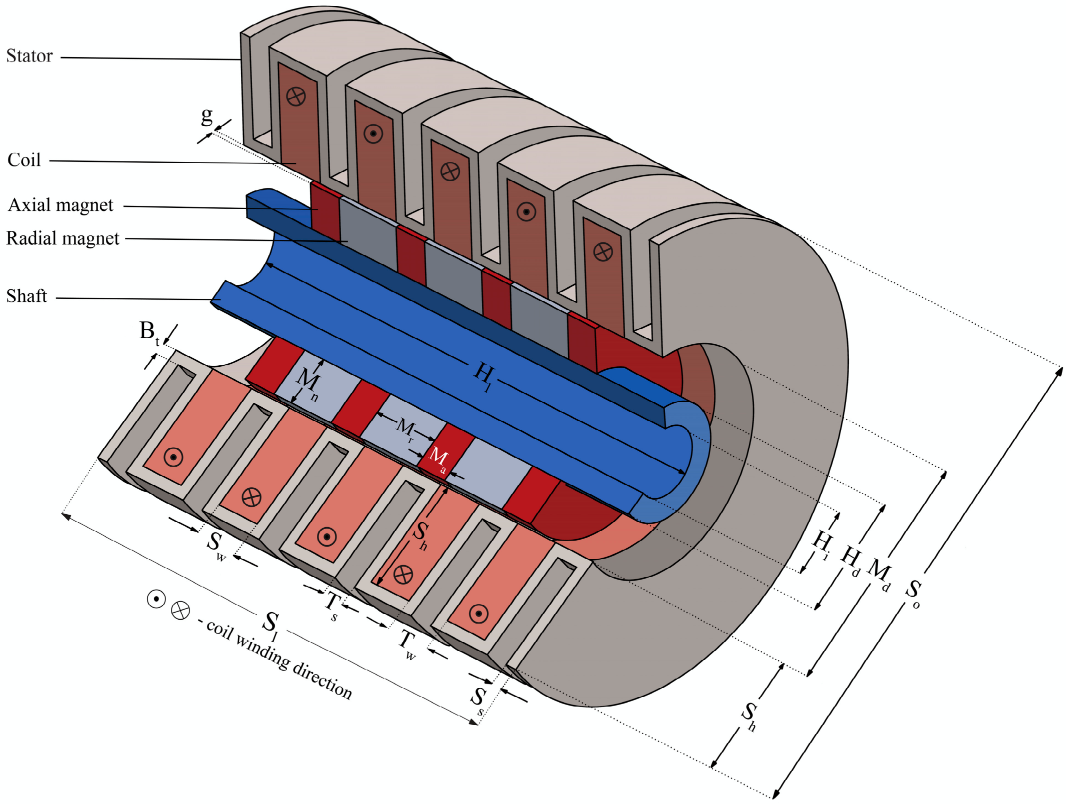

Figure 1. Cut-section view of the slot-spaced linear alternator.

2.2. Grid Independence Check

To ensure the invariance of results for the simulation cases, a grid independence check is carried out to make sure the resultant value converges with decreasing mesh size. A static analysis is carried out with the cogging force to be near zero as a gauging factor. A set of five grids with 169,129, 382,054, 825,167, 1,207,221, and 1,398,177 elements are generated. Figure 2 indicates that the cogging force converges to zero with element number 1,398,177 having −0.0257 N, whereas element number 1,207,221 has −0.0263 N. The difference between the latter two meshes is only −0.0006 N. The trade-off between the computation size and accuracy, the mesh size with 1,207,221 elements is chosen for the simulation cases hereon.

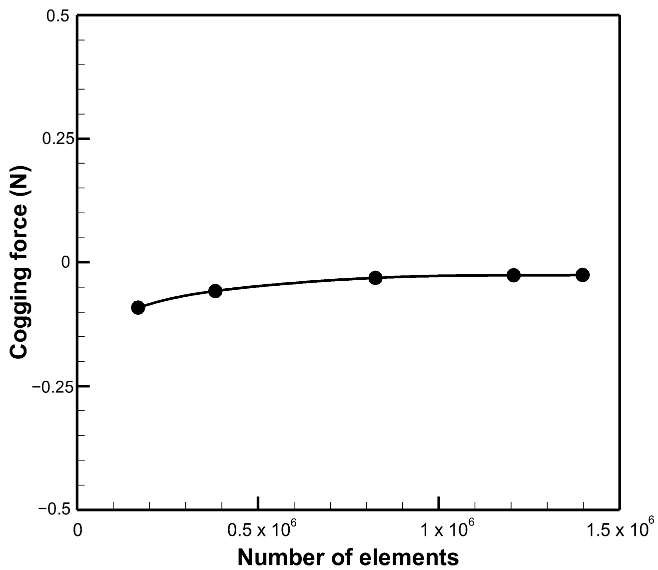

Figure 2. Grid independence check.

2.3. Baseline Case

The finite element analysis for all the simulation cases mentioned is carried out using commercial software, JMag Designer V18. The numerical simulation for the baseline case is carried out to understand the influence of change in geometrical parameters on each part over the cogging force levels and profile. Hence, all parameters are kept to the original form to understand the changes made at a minute level. Even a minuscule change has an impact on the induced voltage and cogging force. The gauging factors of this study are based on these two aforementioned parameters.

The operating condition of the machine for the baseline case is 60 Hz frequency and 5 mm stroke. The baseline case is carried out in both closed- and open-loop conditions. The output voltage and cogging force are measured in a no-load open-loop condition. To determine the rated power of the machine, a 100 Ω purely resistive load is connected in series with a closed-loop condition. The simulation case is divided into 100 steps for one cycle of displacement. Figures 3 and 4 show the contour and vector plot of the magnetic flux density in the original model for the baseline case. To show the characteristic of the cogging force profile, it is compared with the displacement profile and induced voltage in Figure 5. It can be seen that the profile is close to sinusoidal but has an imperfection in the center dead point. Hereon, all the numerical values mentioned induced voltage, cogging force, and power are the Root Mean Square (RMS). With the no-load condition, the cogging force and induced voltage are 146.9 N and 301.9 V, respectively. With the closed-loop condition, the rated power of the machine is 96.9 W.

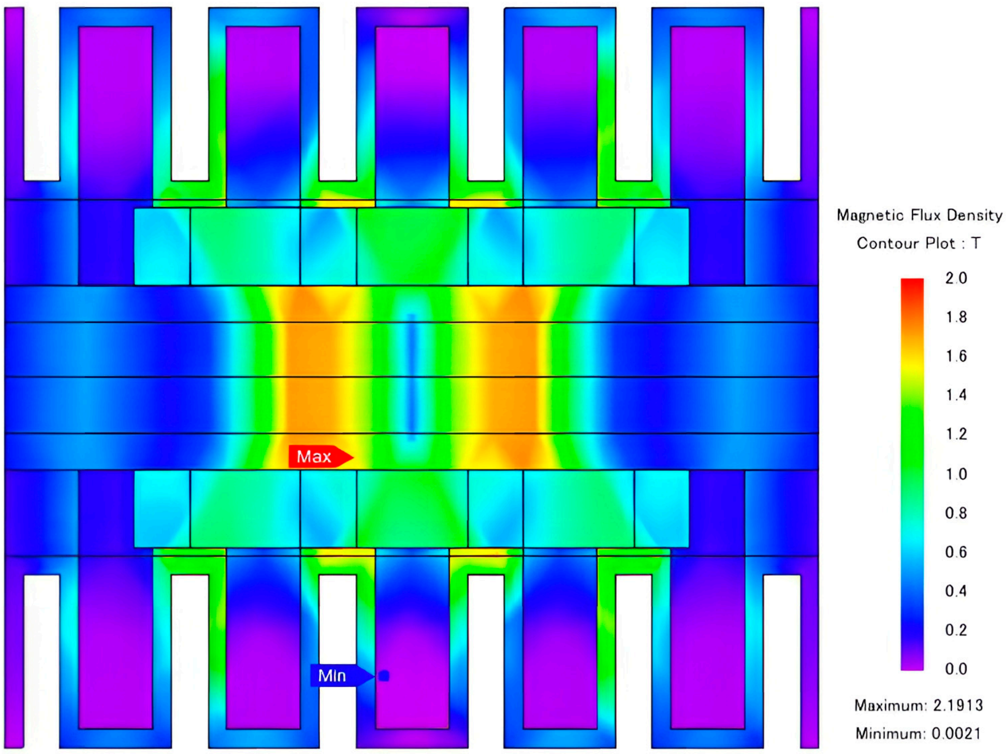

Figure 3. Contour plot of magnetic flux density in a cut-section view of the PMLA for the baseline case.

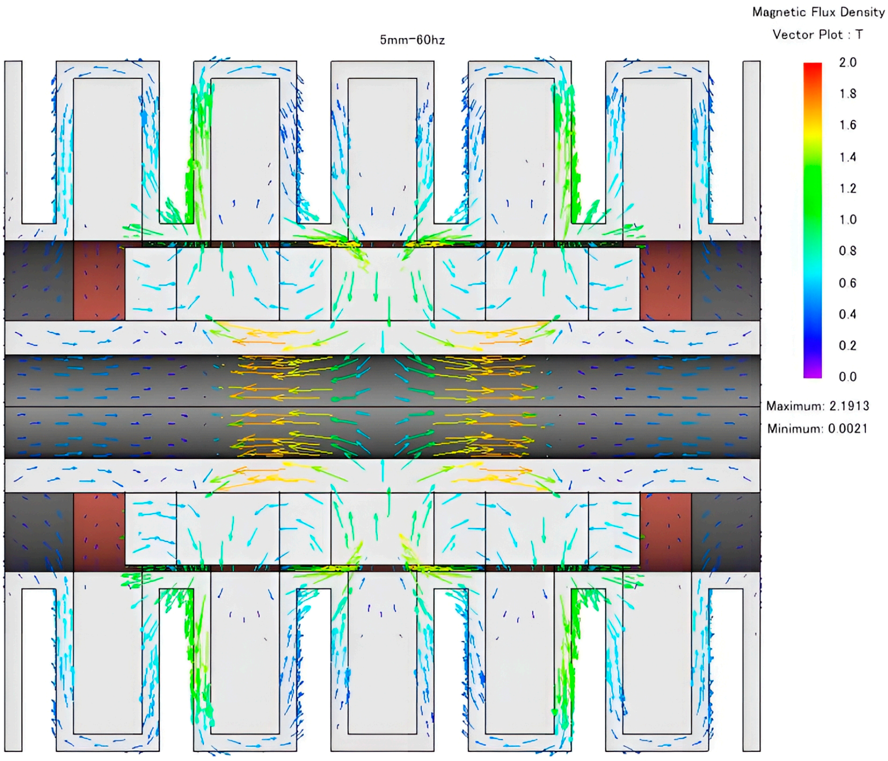

Figure 4. Vector plot of magnetic flux density in a cut-section view of the PMLA for the baseline case.

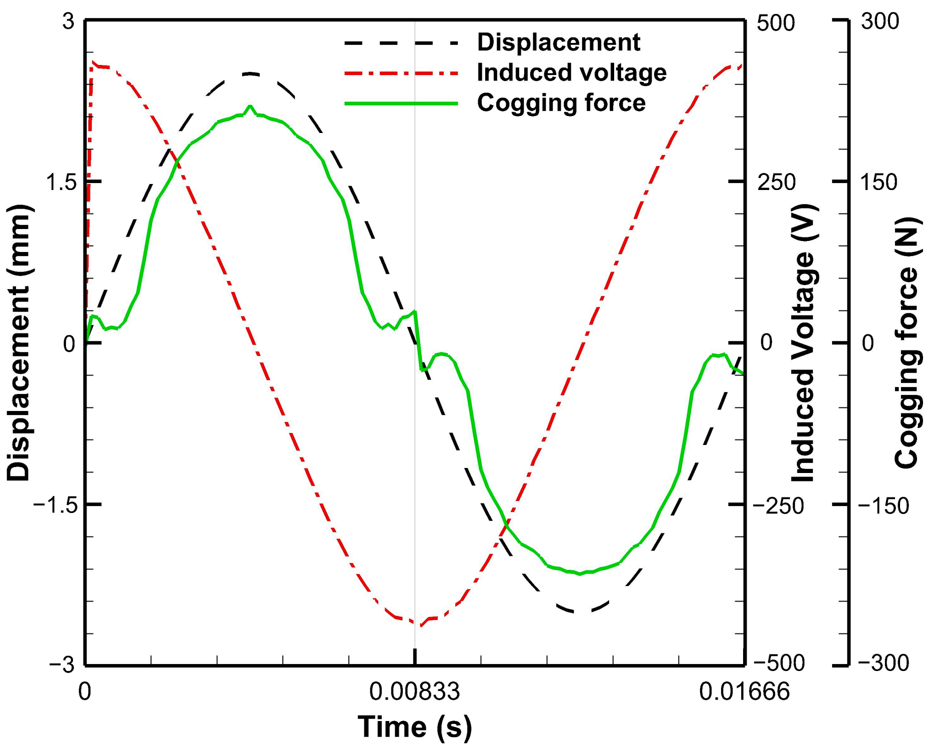

Figure 5. Performance of the PMLA in the baseline condition.

3. Cogging Force and Limitation Methods

3.1. Influence of Geometrical Parameters on Cogging Force

The major drawbacks of the cogging force on PMLAs, other than performance, are damage caused to the machine itself, disturbing of the integrity of the stator build, noise created while operating, and obsolete vibration on the translator. The geometrical parameters of the PMLA have a strong influence over the profile and quantity of the cogging force. The air gap in between the stator and translator is another influential characteristic of the PMLA. An equilibrium needs to be maintained between induced voltage and cogging force with a median air gap. The air gap flux φ_g is given by Equation (1):

$$\varphi_g = B_r \frac{h_m s}{h_m + g} \tag{1}$$

where B_r is remanence, S is the area of permanent magnet magnetization, g is the air gap, and h_m is the permanent magnet magnetization length. Cogging force F can be expressed by

$$F = -\frac{1}{2}\varphi_g \frac{\partial R}{\partial z} \tag{2}$$

where R is reluctance in the air gap and z is translator displacement. The surface of contact between the magnet poles and stator teeth affects the cogging force. Without significantly changing the design elements of the PMLA, there are other methods to reduce or modify the profile of cogging force.

3.2. Assumptions and Conditions

To obtain a modified model with conditions matching the primary motivation of the study, a few conditions and assumptions are considered in the process of geometrical and topological changes to be made in this study.

1. The induced voltage is the primary reflection of the performance of the machine to estimate the efficiency. In the process of reducing the cogging force, the reduction in induced voltage is inevitable in some of the alteration methods. Hence, the variation in parameters of each adaptation is carefully accounted for with the data from cogging force and induced voltage and represented in a graphical form, through which the most reasonable parameter is selected, which maintains equilibrium by not losing the induced voltage and by a significant reduction in the cogging force;
2. The selected parameter which maintains an equilibrium should also hold the cogging profile close to the displacement profile (sinusoidal). If it does not, then the next parameter closely resembling the profile is selected;
3. The alteration methods are close to novelty and cannot be adapted to the traditional packaging techniques of the stator;
4. Major dimensional parameters such as the outer diameter So, tooth width T_w, and the stack length S_l for stator, and pole width M_r, M_a, and thickness M_n of both axial and radial magnets, are unchanged in the alteration process;
5. Some of the considered alteration methods may harm the motivation of the study. Such methods are ignored in the final modified model;
6. Novel alteration methods, such as chamfering of the stator, are difficult in current stacking methods for the stator lamination process. Three-dimensional printing of the parts will make such alterations possible in the foreseeable future.

4. Geometrical Alterations

The design phase of a PMLA is crucial to the marginal elimination of the cogging force. This slot-space model is designed to have maximum power density [16]. Many design alterations are inherited in this study without losing much on the power density factor.

Variation in the air gap vastly decreases the cogging force and so compromises the induced voltage. Skewing of the slots was impractical for toroidal windings in a tubular topology. Semi-closed slots nearly diminished the cogging force, but made another impractical condition for current packaging techniques for the stator [18]. The sloping of magnets has a significant effect on the reduction of the cogging force. Changing the shape of the magnet by creating a wedge-shaped slope on the height creates a smoother surface of flux to flow through the stator, thus having lower friction on the translator [13].

Skewing the magnets has an impact on cogging force, but increases the cost and difficulty in manufacturing [19]. The addition of an assistant tooth has an effect in eliminating the end effect and emptying a slot, but adds to the overall mass of the machine and thus affects the performance figures. Chamfering of the teeth on the other hand has an impact on the cogging force [20]. The effect of notching on the stator tooth has a significant effect on the cogging force, more than the assistive tooth [21].

Considering all implementations, each case of alterations with incremental parameters is numerically studied and compared to the original model graphically. The cogging forces of the parameters close to the promising parameters are closely monitored to match the profile of the displacement. The best parameter is chosen in each category of alteration to build the modified model which has the sinusoidal profile and reduced cogging force. Even a small level of imperfection corrections in the design phase could lead to the benefit of a vital boost in important parameters [22]. Hence, all parameters are carefully monitored and changed.

4.1. Stator Tooth Chamfering

The stator tooth is planar and unaltered in the original model. Chamfering of the stator tooth has a significant effect on the cogging force [21]. The chamfering radius of curvature is increased from 0.25 mm to 2.25 mm in multiples of 0.25. Figure 6 shows an illustration of the chamfering on the stator tooth. The chamfering makes the magnetic flux density flow through the walls of the stator seamlessly and creates less friction in the process. Thus, the profile becomes smoother and approaches sinusoidal down the line from 0 mm to 2.25 mm. Adversely, the level continues to rise from 1 mm as the surface area of contact is significantly reduced. Unlike cogging force, the induced voltage reduces from 306.7 V to 298.9 V. The cogging force is near constant between 0.25 mm and 1.00 mm at 128 N average. Beyond this region, it continues to raise and peaks at 195.5 N, with a 2.25 mm chamfering radius of curvature. This could be seen in Figure 7, which shows the influence of chamfering the stator tooth on cogging force and induced voltage. Although the 0.75 mm chamfering radius provides the lowest (127.3 N) cogging force compared to the neighboring values, the profile is the second important candidate to choose the preferred value of chamfering radius. Hence, Figure 8 shows the profile of cogging force for 0.75, 1, and 1.25 mm, where 1 mm is closer to sinusoidal than other values. Also, the induced voltage for 0.75 mm is 302.24 V and for 1 mm is 302.2 V. The trade-off is close, and a 1 mm radius of curvature for chamfering is the chosen alteration value for this case.

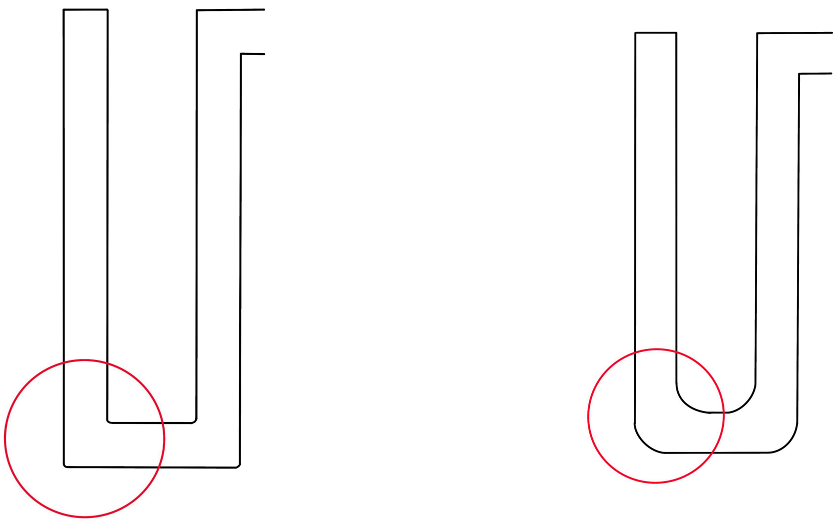

(**a**) (**b**)

Figure 6. Chamfering radius on stator tooth (**a**) 0.25 mm and (**b**) 2 mm.

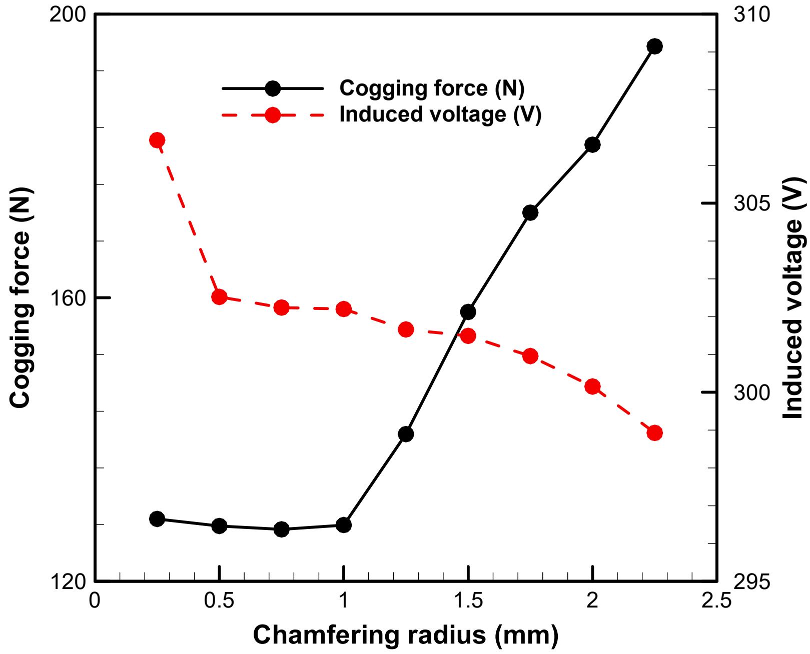

Figure 7. Influence of stator tooth chamfering on cogging force and induced voltage.

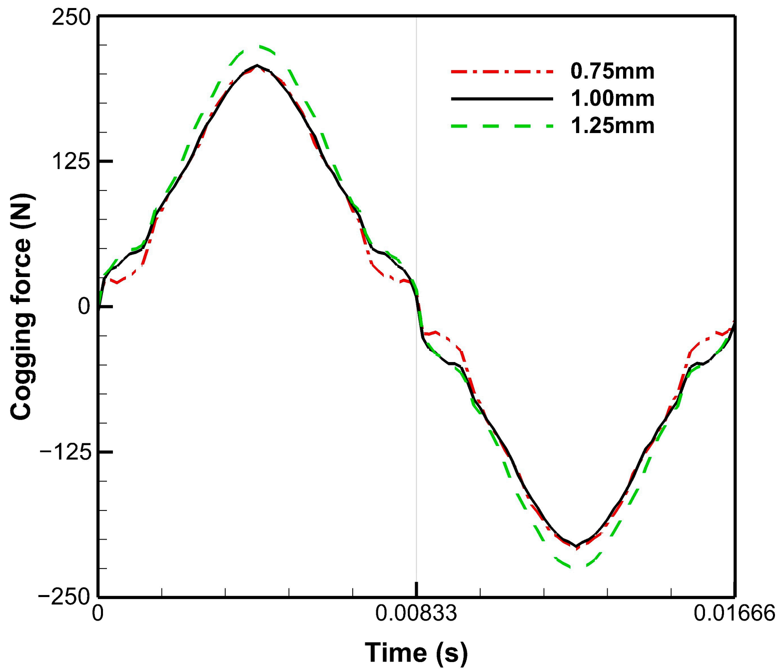

Figure 8. Comparison of cogging force profiles with the chamfered stator tooth.

4.2. Magnet Chamfering

Chamfering of the magnets increases the surface area of contact with the stator tooth and reduces the end effect caused. The original planar magnets produce 146.9 N of cogging force at 301.9 V induced voltage. The chamfering radius of curvature is increased by a multiple of 0.25 mm in this study. Figure 9 illustrates the difference between chamfering with a 0.25 mm and 2 mm radius of curvature for both the axial and radial magnets. By the introduction of 0.25 mm chamfering, the cogging force drastically reduced to 119.3 N with 303.896 V. The induced voltage rose with a reduction in the cogging force, which is unseen and an attractive candidate to consider. Figure 10 shows the change of profile with an increased chamfering radius. The reduction in cogging force gradually reduces to 115.1 N at 0.75 mm, with the highest induced voltage of 306.1 V. Beyond the 0.75 mm region, the profile of the cogging force raises beyond the planar model to a maximum of 164.8 N at a reduced induced voltage of 300.5 V. This change shows a clear indication that the preferred value of chamfering is 0.75 mm. The profile of the cogging force with 0.5, 0.75, and 1 mm also reflects the same in Figure 11. The profile comparison between 0.75 and 1 mm shows that 1 mm has the clear advantage of being more sinusoidal but produces elevated cogging force. Apart from chamfered magnets, there are other candidates to consider, and they bring further changes to the final modified model. Hence, 0.75 mm is chosen to be the best value for chamfered magnets, due to the lowest cogging force produced in these variations.

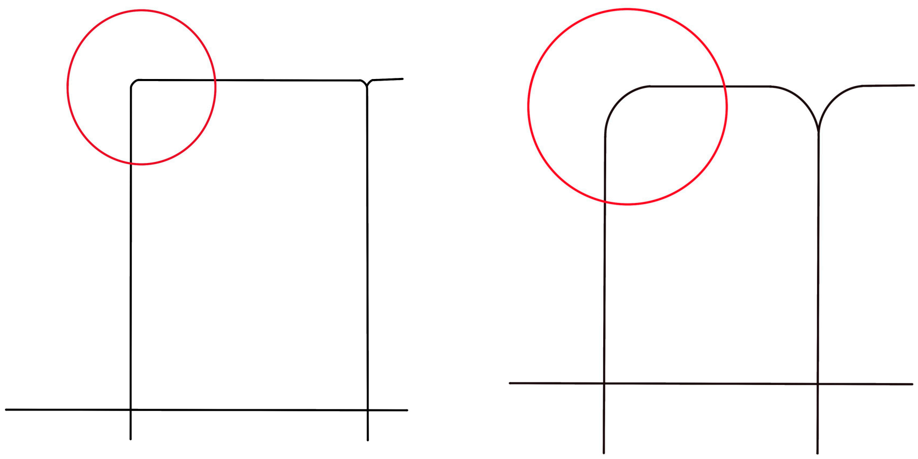

(a) (b)

Figure 9. Chamfering radius on magnets (**a**) 0.25 mm and (**b**) 2 mm.

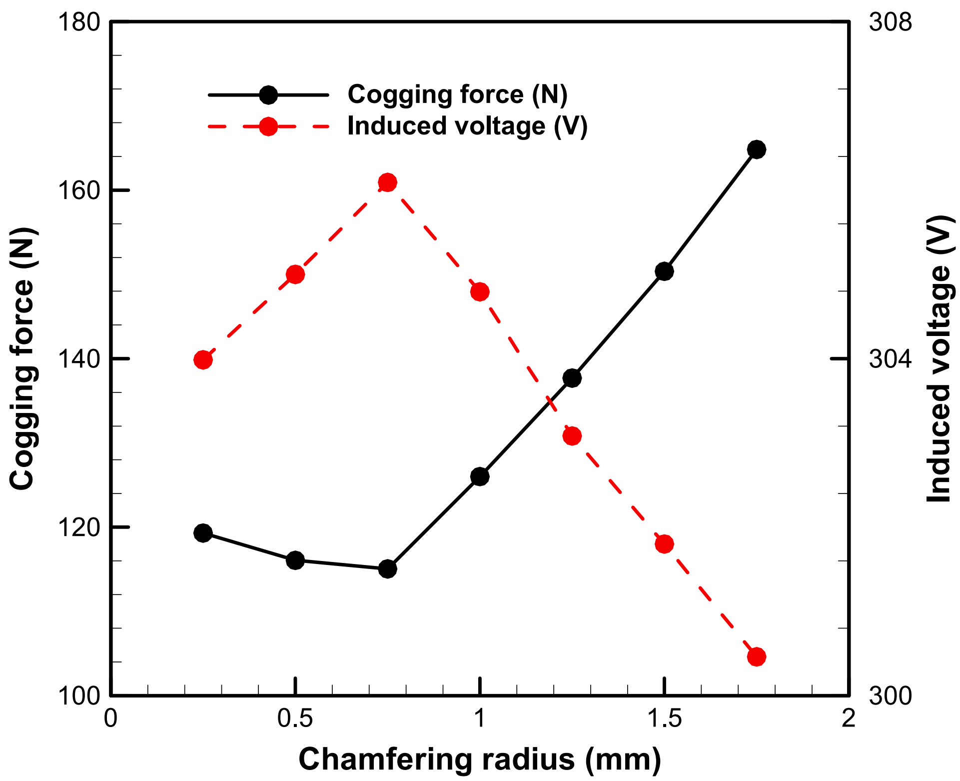

Figure 10. Influence of chamfered magnets on cogging force and induced voltage.

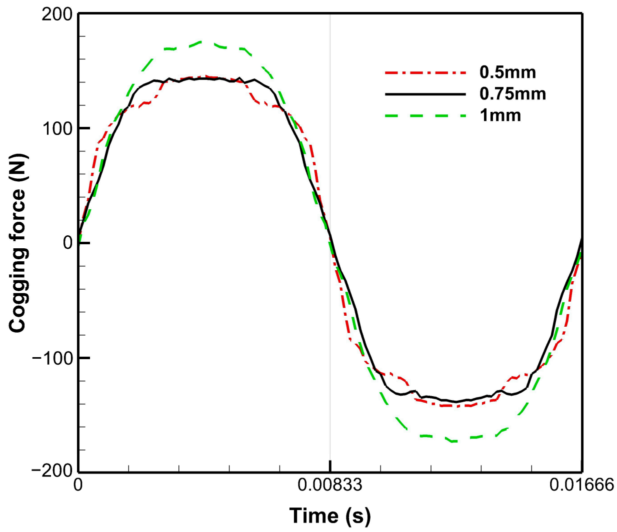

Figure 11. Comparison of cogging force profile between 0.5, 0.75, and 1 mm chamfering radius of curvature.

4.3. Tooth Elimination

The slot-spaced PMLA has a six-tooth tubular structure. End teeth are eliminated instead of adding an assistive tooth to reduce the cogging force and add to the overall mass of the machine. In the four-tooth model, as shown in Figure 12, the overall mass of the machine is lighter by 10% and increases the overall power density of the machine. However, the gain is not significant. Figure 13 shows a comparison of four- and six-tooth models. The original six-tooth model produces an induced voltage of 301.9 V with 146.9 N cogging force, and the four-tooth model, on the other hand, produces 292.2 V of induced voltage and 142.9 N of cogging force. The loss in cogging force is in the same ratio as the induced voltage. Figure 14 also illustrates the profile of the cogging force for both models, and they are the same, with the four-tooth being lower than the six-tooth. The profile and the overall trade-off between induced voltage and cogging forces are not significant. Hence, this modification is not a significant candidate to consider.

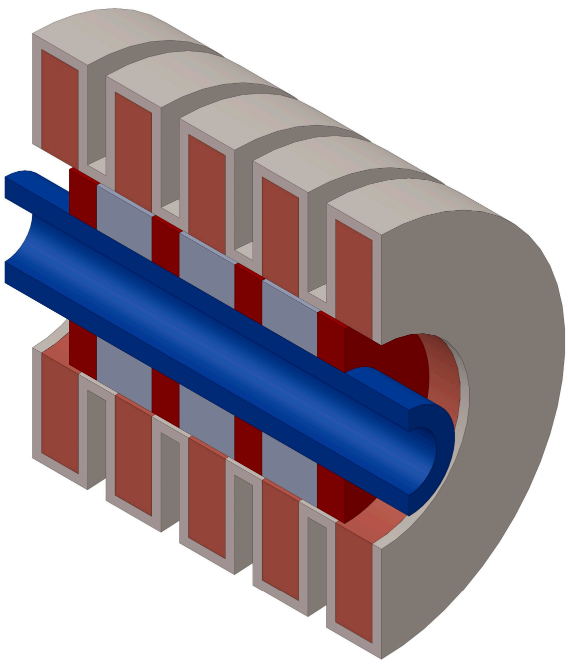

Figure 12. Cut-section view of the four-tooth model.

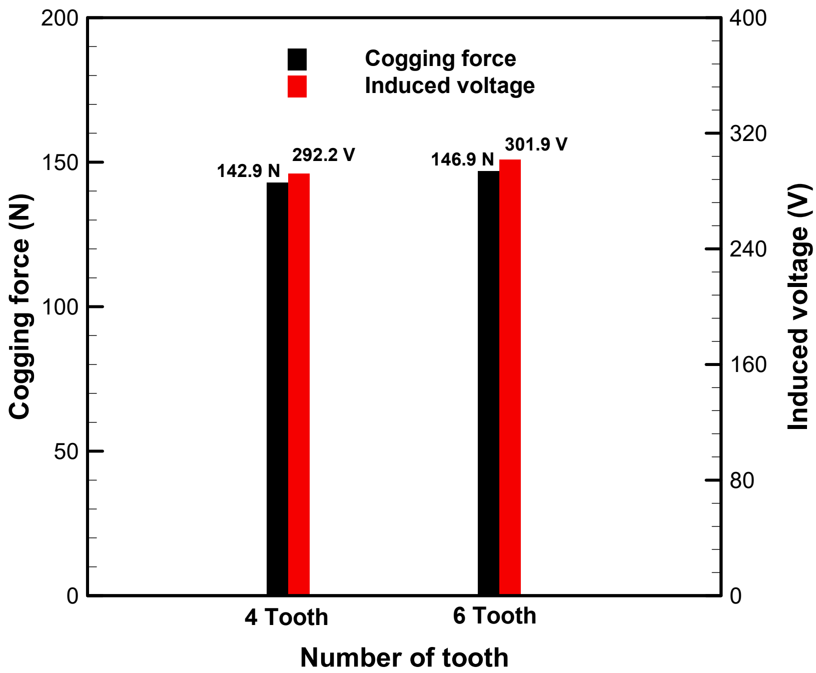

Figure 13. Comparison of induced voltage and cogging force for four- and six-tooth models.

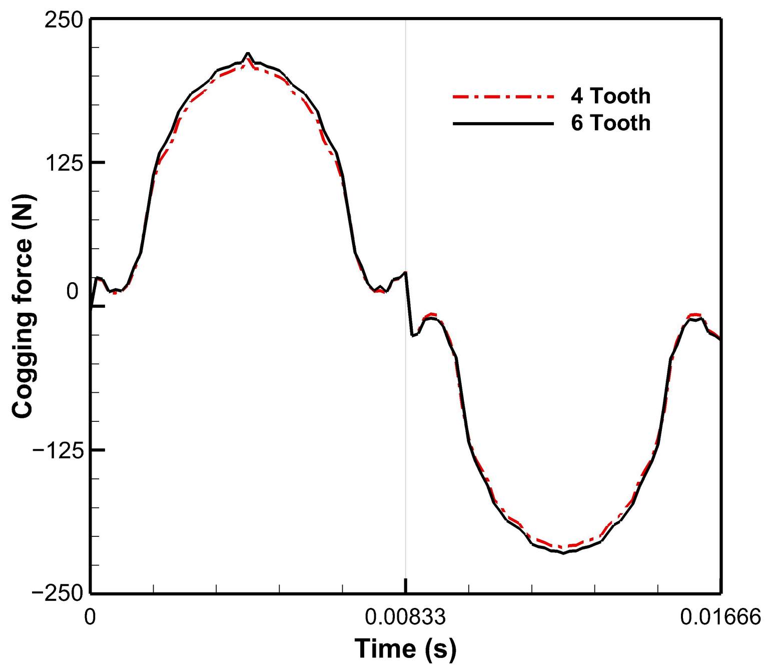

Figure 14. Comparison of cogging force profile between four- and six-tooth models.

4.4. Axial Stator Notching

Creating a bulging valley facing downwards makes a notch on the tooth. The notch is made on the top and bottom sides of the tooth. The top faces the magnets and down in the slot space. The tooth width Tw is 5 mm and, to increase the surface area within a short space, notching is a significant candidate. The flat plane of the tooth is close to a circumferential patch in a 35 mm radius of curvature. Hence, a reasonable 30 mm notching radius of curvature is considered for introduction to this study. Decrementing the radius of curvature step by step with a multiple of 2.5 mm to 15 mm is chosen to perform an analysis. Figure 15 shows the illustration of notching in 27.5 and 15 mm models. Any value beyond

30 mm is planar and any less than 15 mm is impractical in the lamination process of the stator. The structural integrity of the stator is critical below this region.

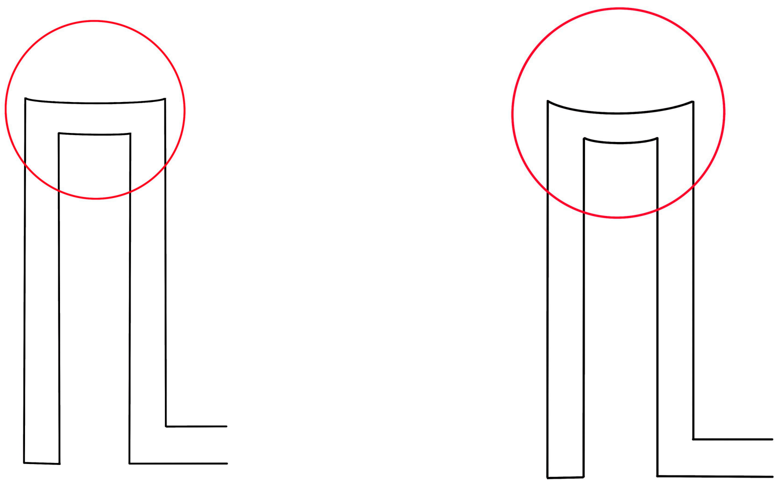

(**a**) (**b**)

Figure 15. Axial stator notching with a radius of curvature (**a**) 27.5 mm and (**b**) 15 mm.

Figure 16 shows the influence of notching on the stator in the axial direction over induced voltage and cogging force. The flat plane tooth in the original model produces a cogging force of 146.9 N. Comparatively, the 30 mm notching radius produces a lesser cogging force of 105.8 N with 296.2 V of induced voltage, through to a 15 mm notching radius producing 96.3 N of cogging force and 281.1 V of induced voltage. The notching radius of 22.5 mm provides a reasonable trade-off value between the induced voltage and the cogging force with 288.1 V and 99.3 N, respectively. The cogging force profile in Figure 17 also proves the same. The neighboring values of 20 mm and 25 mm do not prove to be suitable values fitting the motivation. The chosen value of this modification method is 22.5 mm.

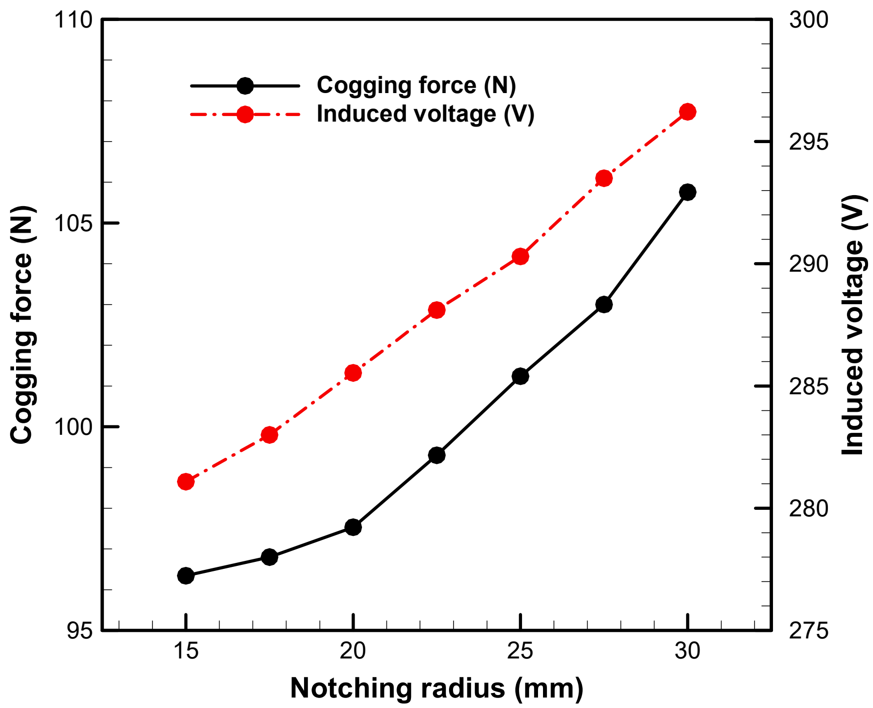

Figure 16. Influence of axial stator notching over induced voltage and cogging force.

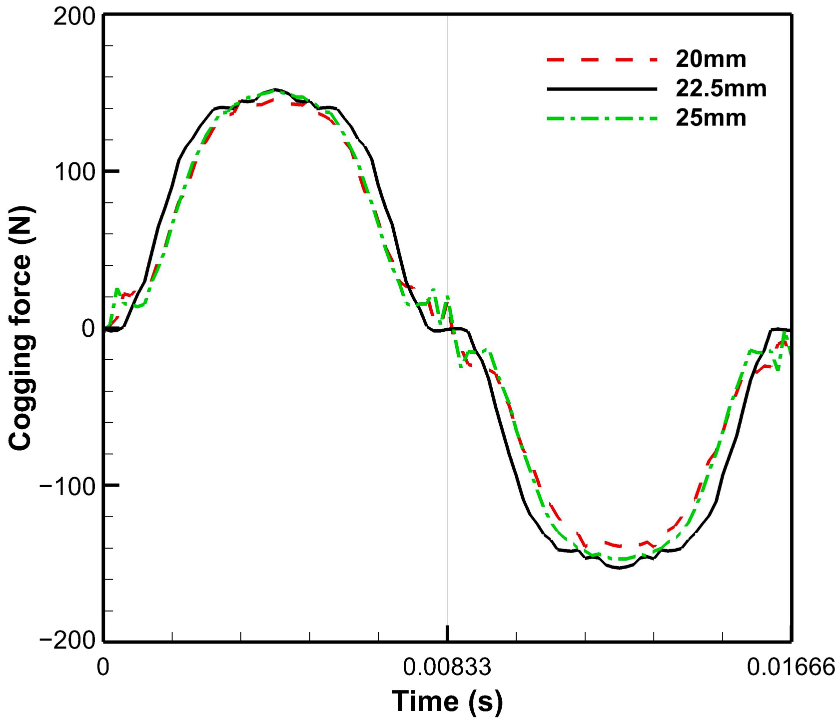

Figure 17. Comparison of the cogging force profile between 20, 22.5, and 25 mm models.

4.5. Axial Magnet Notching

The pole width for axial and radially magnetized magnets are 7.5 and 15 mm, respectively. To increase the surface area similar to the stator, notching on the magnets is made uniformly both on axial and radial magnets. The planar magnet is equivalent to a circumferential patch of a 60 mm radius of curvature. Hence, the notching radius of 60 mm is decreased in multiples of 5 mm to 15 mm. Figure 18 illustrates the difference between the 15 mm and 60 mm notching radius. Any radius less than 15 mm is unconventional for the manufacturing process. Compared to the conventional model, the 60 mm notching radius produces a lower cogging force of 130.2 N with 289.2 V of induced voltage. The lowest case, with a 15 mm radius, produces the least cogging force of 62.1 N with 255.4 V of induced voltage. The influence of axial magnet notching on the cogging force and the induced voltage is shown in Figure 19. With a decrement in the notching radius, the cogging force also falls steeply with the induced voltage, and this is similar to the stator notching. Hence, a median notching radius value of 35 mm is selected to set an equilibrium between key factors, although, to confirm the type of cogging force profile, it is compared with 30 and 40 mm cases. This is clearly illustrated in Figure 20. Although the 40 mm case has a clear sinusoidal profile, the 35 mm case is considered better and with further investigation of other factors, this sinusoidal profile is met. Hence, the selected value from this modification method is 35 mm.

4.6. Radial Stator Notching

The inner diameter Md of the stator is 46 mm and the back iron thickness Bt is 5 mm. To introduce notching in the radial direction, an optimal level of depth should be chosen without affecting the back-iron thickness which, in turn, does not affect the structural integrity of the stator. From a design perspective, 14 mm from the origin, a circumferential patch with a 9 mm radius of curvature makes M_d from the original model. Hence, incrementing with 0.1 mm to 10 mm, a radial notch is developed on the tooth of the stator. To maintain a uniform gap throughout the tooth and not overlap on the inner surface, 10 radial notches are introduced per tooth. Figure 21 shows the radial notch in the stator for a 9.5 and 10 mm radius of curvature without any overlap.

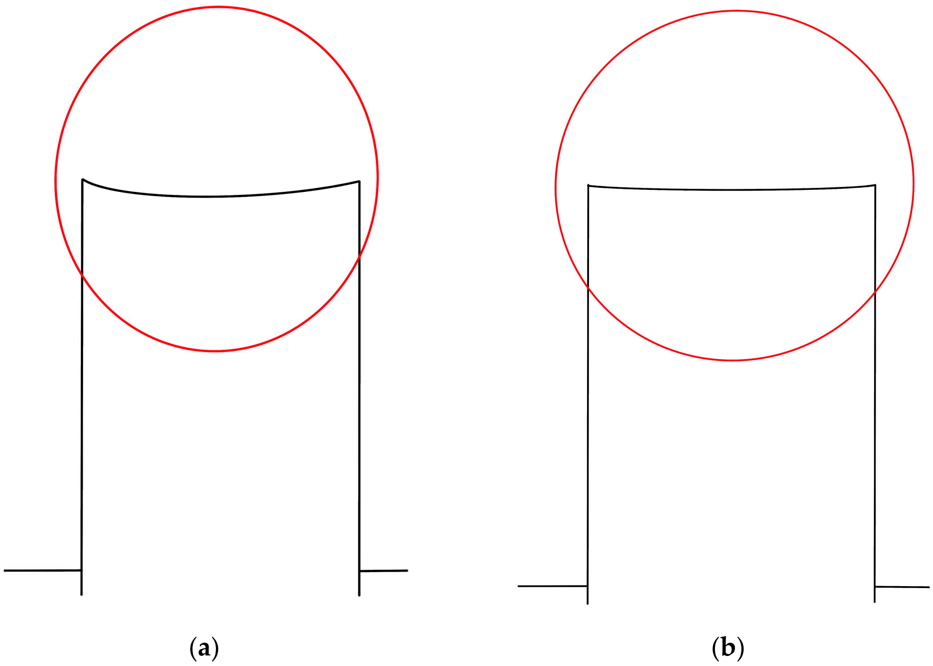

Figure 18. Axial magnet notching radius of curvature (**a**) 15 mm and (**b**) 60 mm.

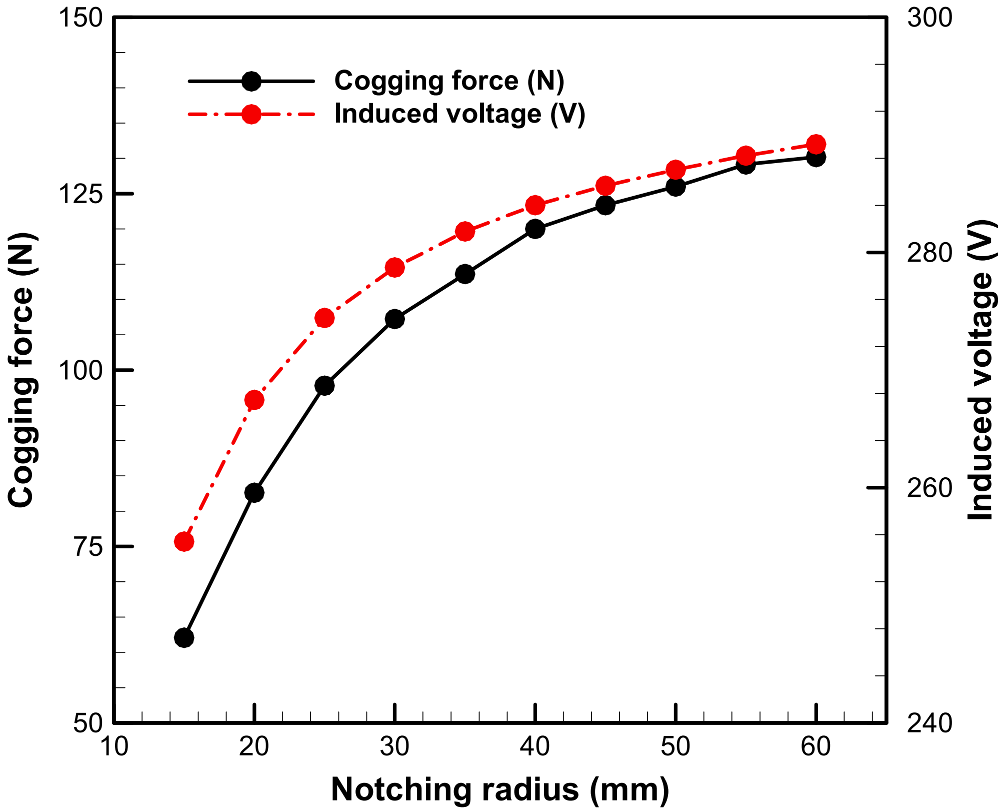

Figure 19. Influence of axial magnet notching over induced voltage and cogging force.

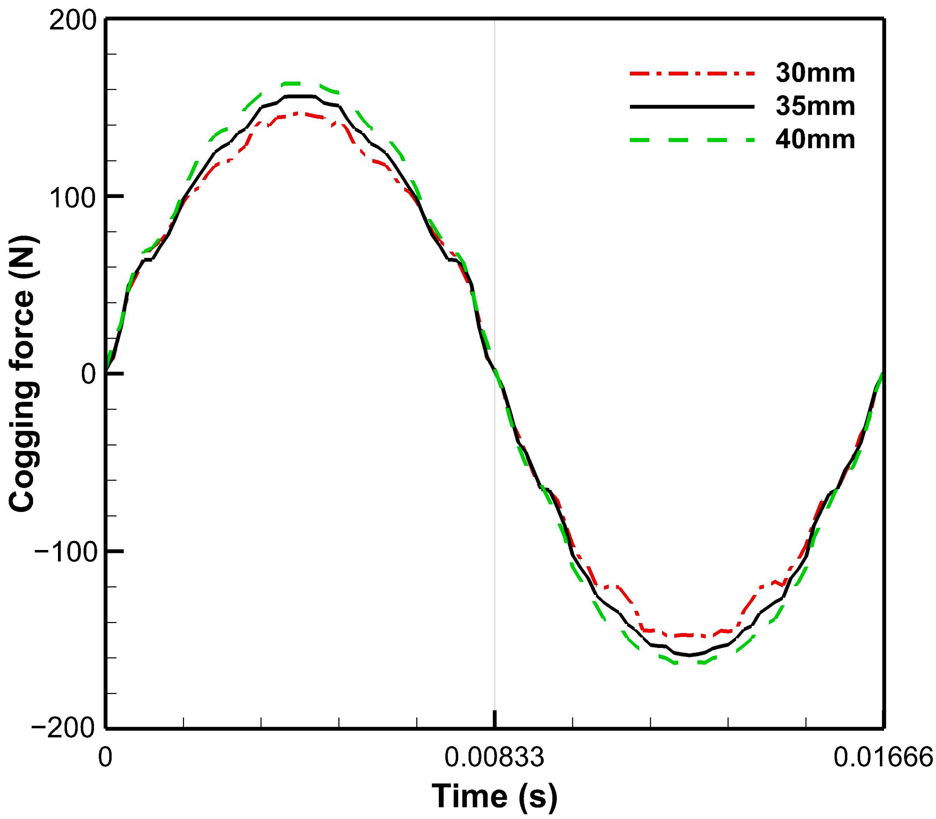

Figure 20. Comparison of cogging force profile with 30, 35, and 40 mm axial magnet notching.

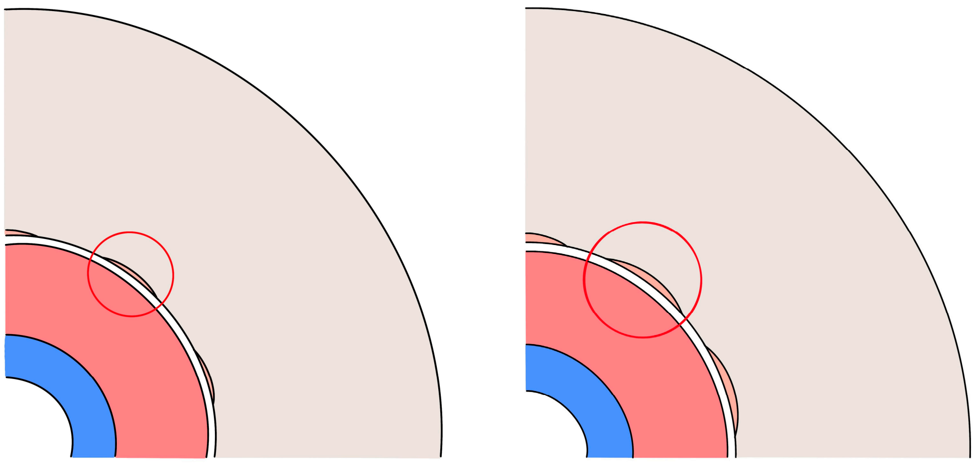

(**a**) (**b**)

Figure 21. Radial stator notching with a radius of curvature of (**a**) 9.5 mm and (**b**) 10 mm.

Considering the cases for analysis, models ranging from 9.1 to 10 mm radial notching are analyzed for changes in key factors of this study. Figure 22 clearly shows the influence of radial stator notching on induced voltage and cogging force. The 9.0 mm case, being the conventional model without notching, makes 146.9 N of cogging force with 302 V of induced voltage. Moving down the line with other cases, the 10 mm notch makes 139.8 N of cogging force with 283.5 V of induced voltage. The 9.4–9.6 mm case prove to be attractive candidates to choose from, providing 141.7, 141.2, and 140.5 N of cogging force with 296.1, 295, and 292.7 V of induced voltage. Their cogging force profile is compared in Figure 23, and a 9.5 mm radial stator notching proves to be an ideal value to choose with a close sinusoidal profile.

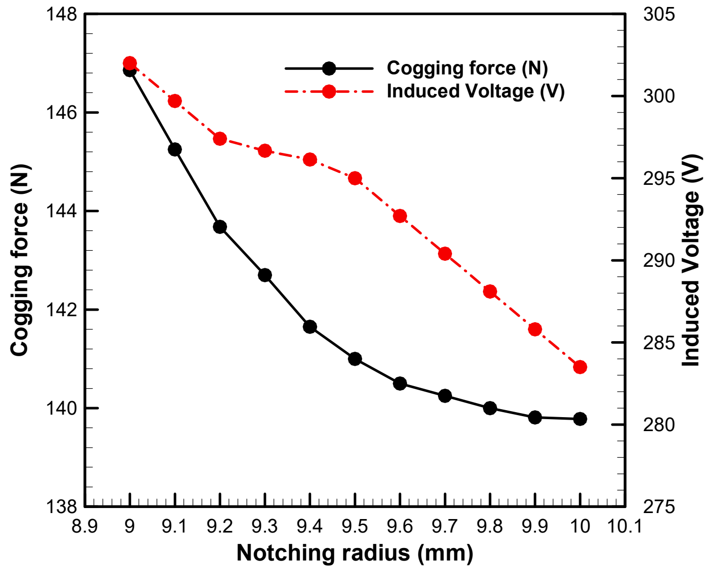

Figure 22. Influence of radial stator notching on induced voltage and cogging force.

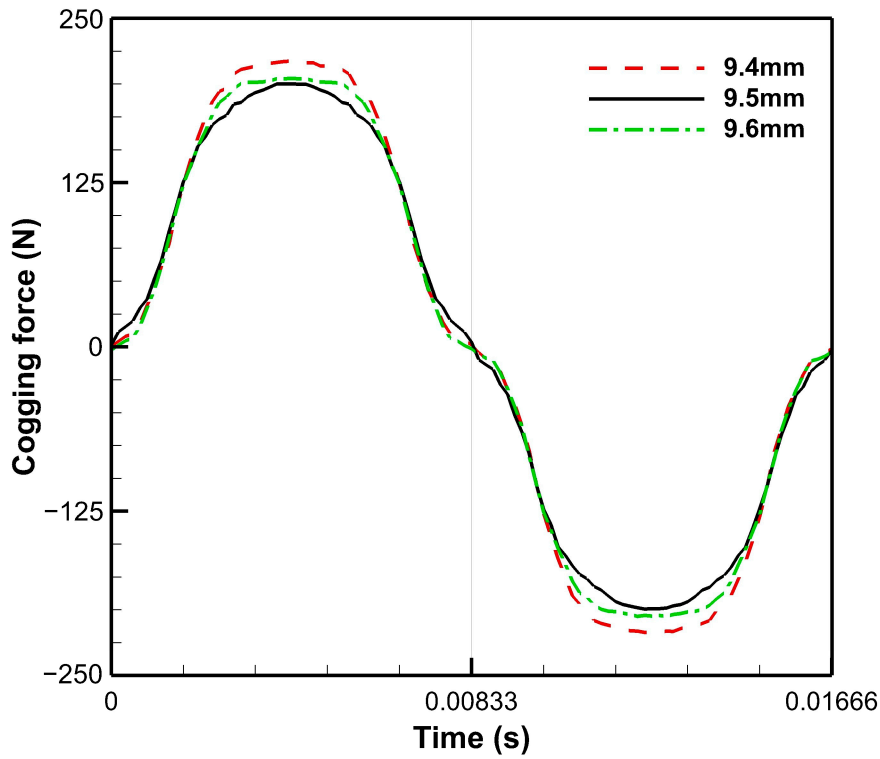

Figure 23. Comparison of cogging force profile for 9.4, 9.5, and 9.6 mm radial notching.

4.7. Type of Stator Notching-End Effect Analysis

The end effect causes elevated levels of cogging force. We choose to not eliminate the end tooth and not add a supportive tooth for the reduction in cogging force. Hence, introducing notching in an alternative manner makes a difference. Two cases of such alteration are made for this study. The first type is to keep the end teeth flat and to make the center tooth notched with a radius of curvature of 27.5 mm. The second type is to only notch tooth numbers 2 and 5 with the same radius of curvature as the first case. Figure 24 shows a clear representation of these cases. The influence of end effect analysis is shown in Figure 25. In comparison with the conventional flat tooth model, the flat end tooth model with all center teeth notched proved to be the better model, making 94.7 N of cogging force with 281 V of induced voltage. On the contrary, the center tooth notched model increased the cogging force to 165.2 N over the conventional model. Hence, the flat-end tooth is the chosen topology to build a modified model from this modification method.

(a) (b)

Figure 24. Type of notching: (**a**) flat end tooth, (**b**) center tooth notched.

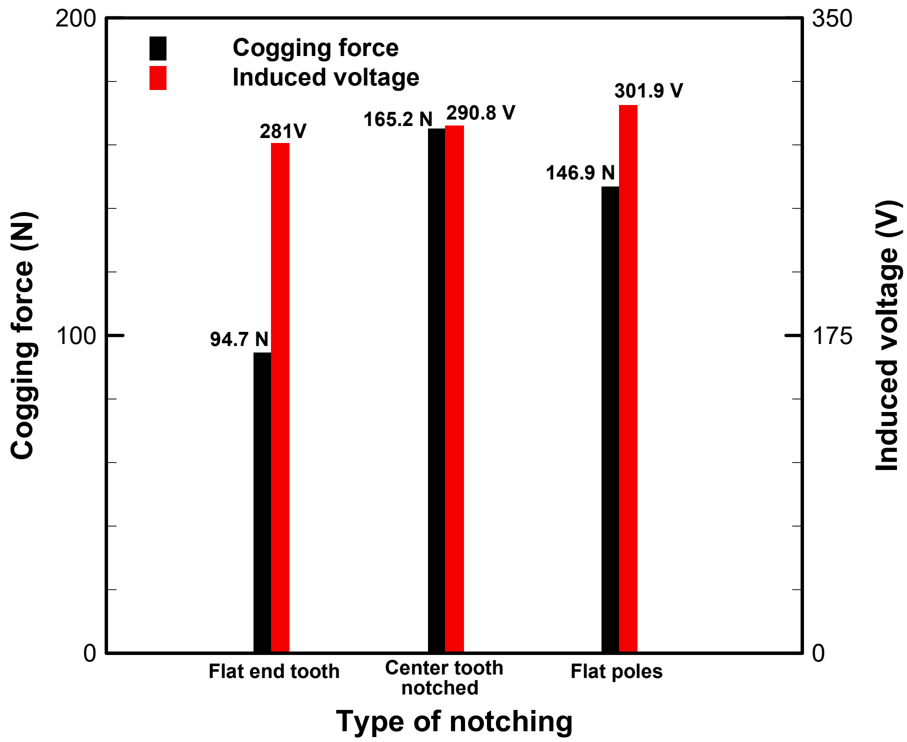

Figure 25. Influence of type of stator notching over induced voltage and cogging force.

4.8. Stator Tooth Ridging

The inversion of a notch with the closest point of the stator to the magnets is the same as the original air gap g, and is a ridge here. Hence, a 15 mm radius of curvature is introduced throughout the stator tooth, and this can be observed in Figure 26. The surface area of contact with the poles to the tooth is still maintained at a 1 mm air gap. The peak point of the ridge maintains this air gap, although the overall surface area of the stator increases the air gap from the poles. Thus, the magnetic flux density distribution around this airgap is weak and creates even more thrust and strain on the translator. The magnetic flux density distribution over one of the center teeth can be seen in Figure 27. With weak flux linkage comes less induced voltage, and the influence of ridging is shown in Figure 28. The ridged model produces 188.9 N of cogging force with 287.7 V of induced voltage. This is 22.24% more cogging force than the conventional model. Hence, ridging would not be considered for the modified model build.

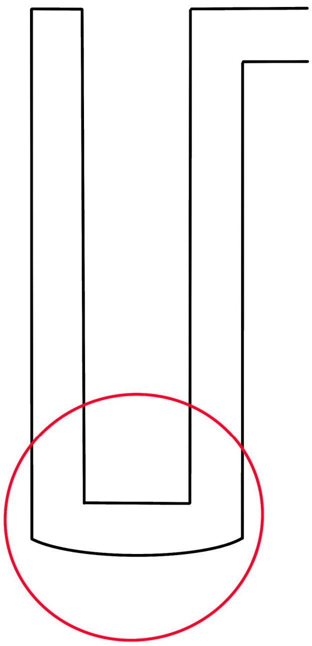

Figure 26. A ridged tooth with a 15 mm radius of curvature.

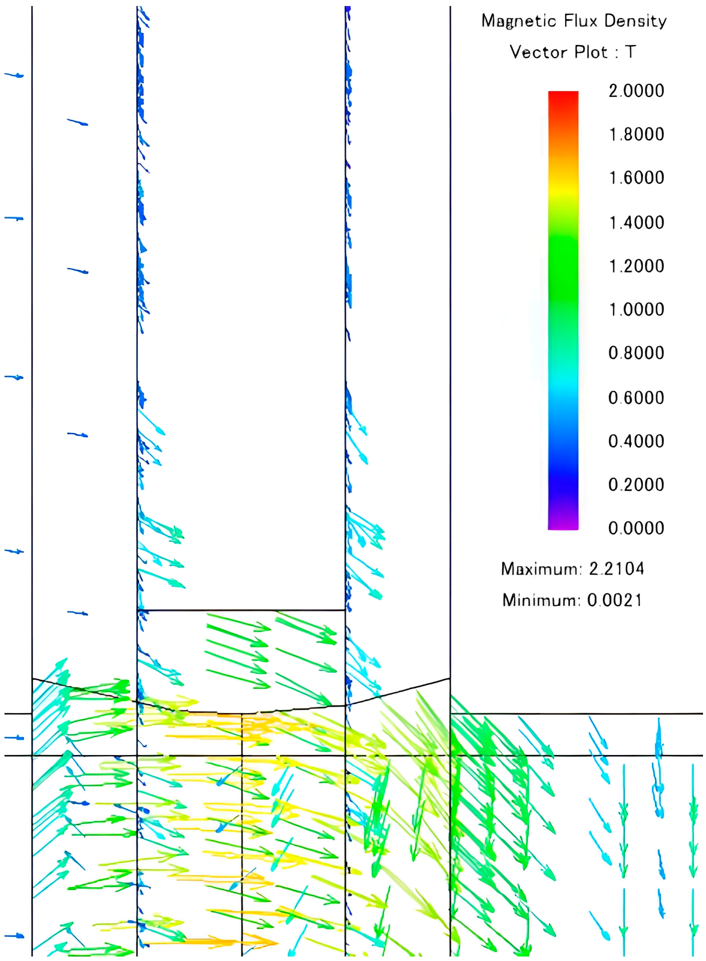

Figure 27. Magnetic flux density in a ridged tooth.

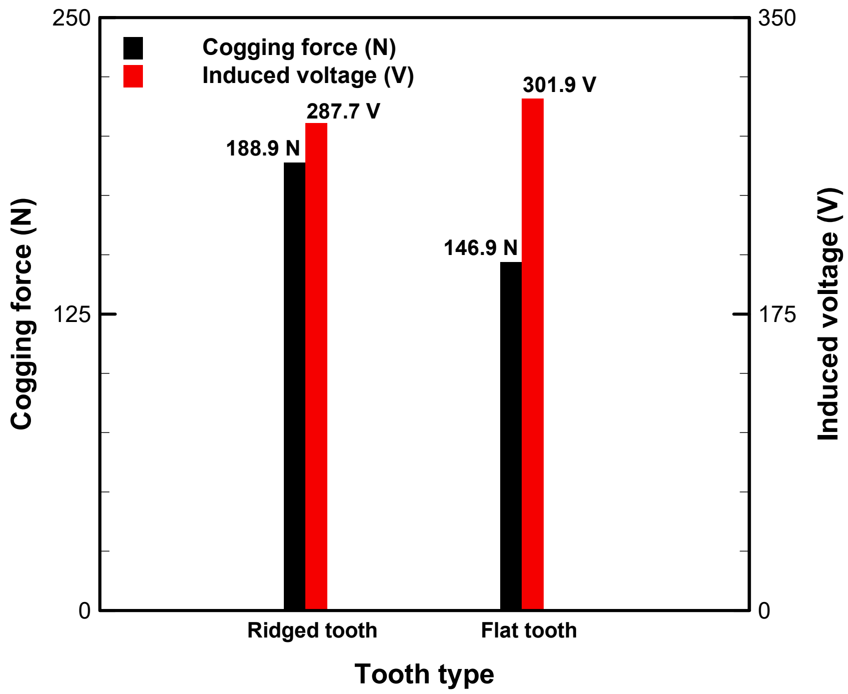

Figure 28. Comparison of cogging force and induced voltage of a ridged model with the original model.

4.9. Magnet Splitting

In pursuit of our experimental model, the customization in producing magnets made us split the magnets into two halves. To study the effects of magnet splitting, we observed the reduction in cogging force in comparison with the original model through the numerical simulation process. Hence, magnet splitting is considered one of the methods in this study. Figure 29 shows the Magnets split into two, three, and four, respectively. The influence of pole splitting on the cogging force is high. From 146.9 N in the conventional model, it gradually reduces to 126.2, 110.1, and 84.3 N for two-, three-, and four-piece poles, respectively, by compromising induced voltage. This comparison can be seen in Figure 30. Though the four-piece model produces the lowest of all cogging forces, the compromise is on induced voltage, which reduces to 69.4 V, and the profile of cogging force is distorted, as seen in Figure 31. The cogging force profile of three- and four-piece models does not resemble a sinusoidal profile, and the compromise on induced voltage is not at a considerate level. The two-piece model, on the other hand, made 126.2 N of cogging force, which is 14.1% less than the one-piece model. Hence, the two-piece pole topology is the selected model in this modification method.

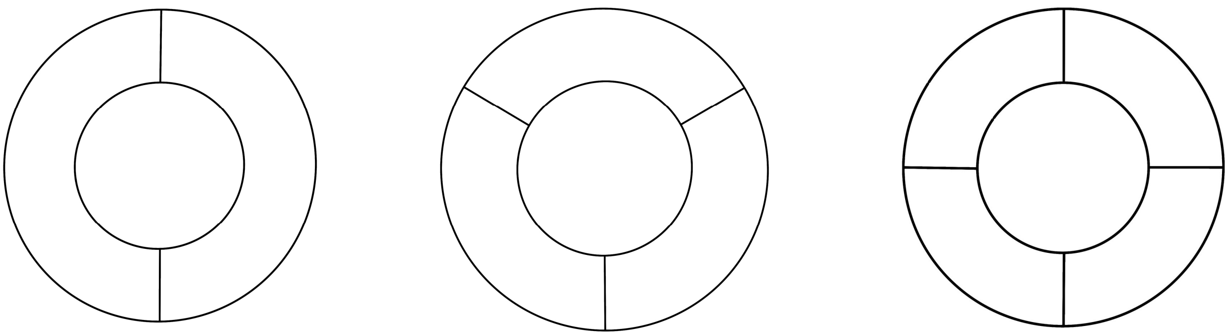

(**a**) (**b**) (**c**)

Figure 29. Split magnets (**a**) two pieces, (**b**) three pieces, and (**c**) four pieces.

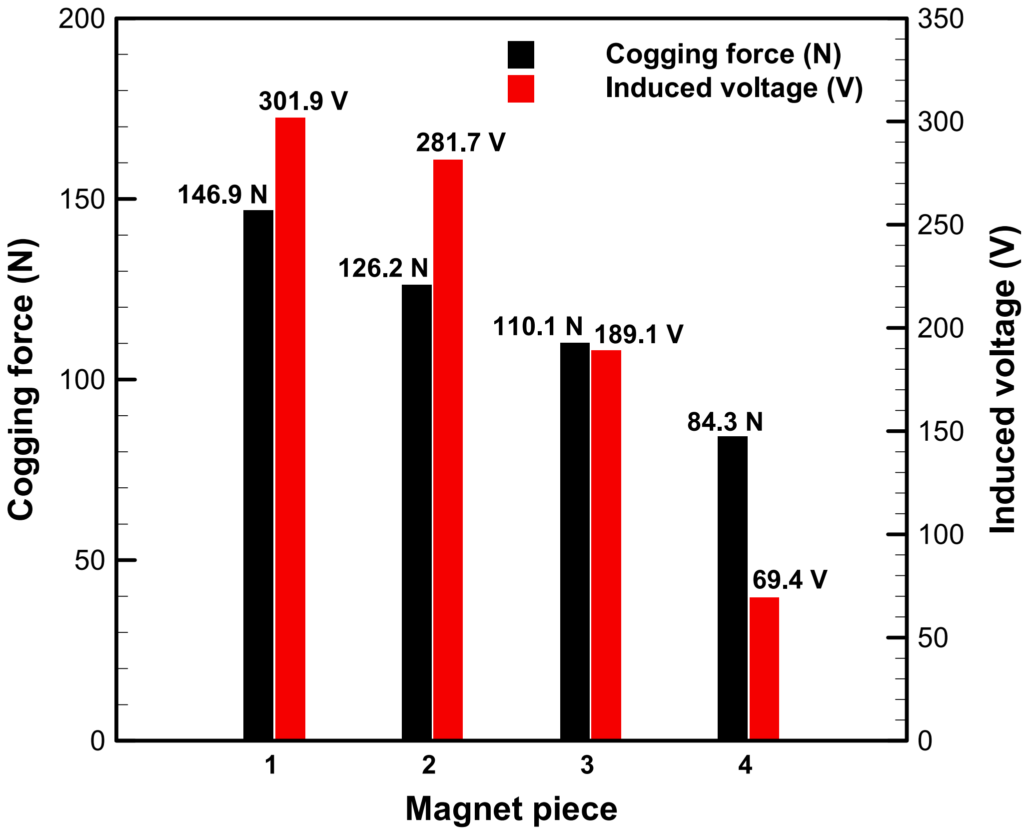

Figure 30. Influence of magnet splitting over induced voltage and cogging force.

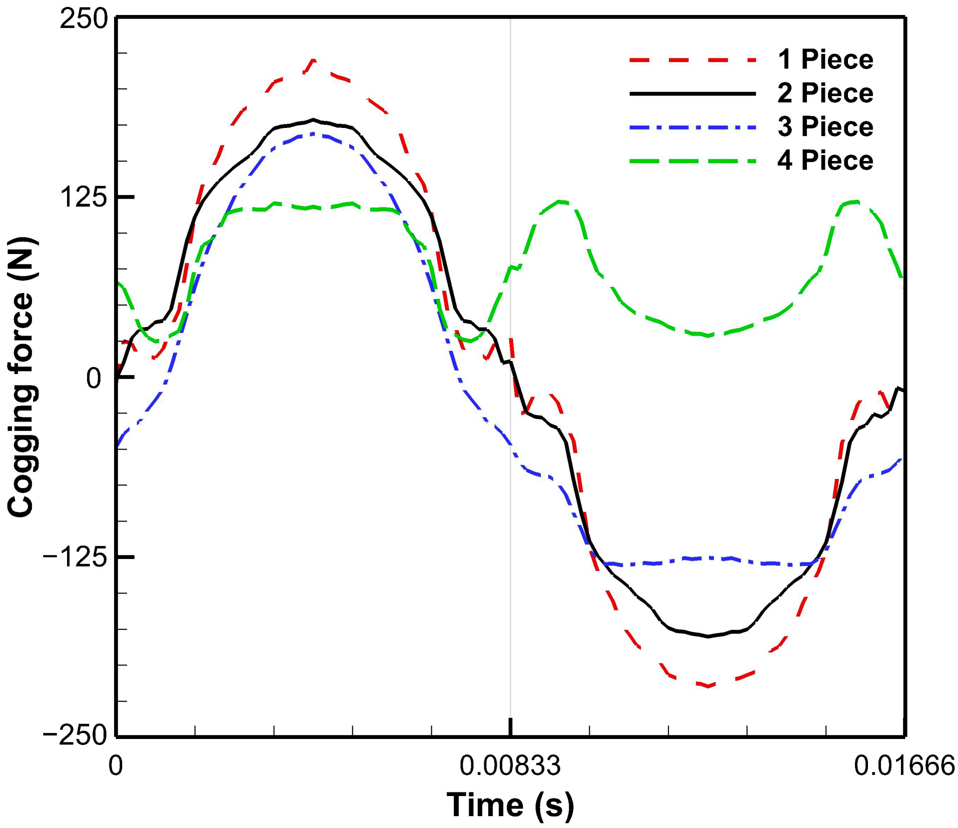

Figure 31. Cogging force profile of 1–4-piece magnets.

5. Modified Model

Considering all the alterations for modification in the original model, Figure 32 shows the illustration of all the implementations on the modified model. Table 2 shows all the geometrical alterations considered for this modified model and their respective values, topology, or parameter. Implementing this model for the numerical simulation, the profile of the cogging force obtained on the translator is in line with the displacement profile of the translator. This can be observed in Figure 33. The RMS cogging force of the modified model is 98.2 N with 281.4 V of induced voltage. Compared with the original model, the cogging force is reduced by 33.15% and the induced voltage is compromised by 6.79%. The comparison of the cogging force profile from the original model and the modified model is illustrated in Figure 34. With a closed-loop purely resistive loading condition, the modified model produces 81.8 W of power. This is 15.6% lower in comparison to the original model. The trade-off is acceptable, and the original goal to produce a sinusoidal profile is met. This comparison is represented in Figure 35.

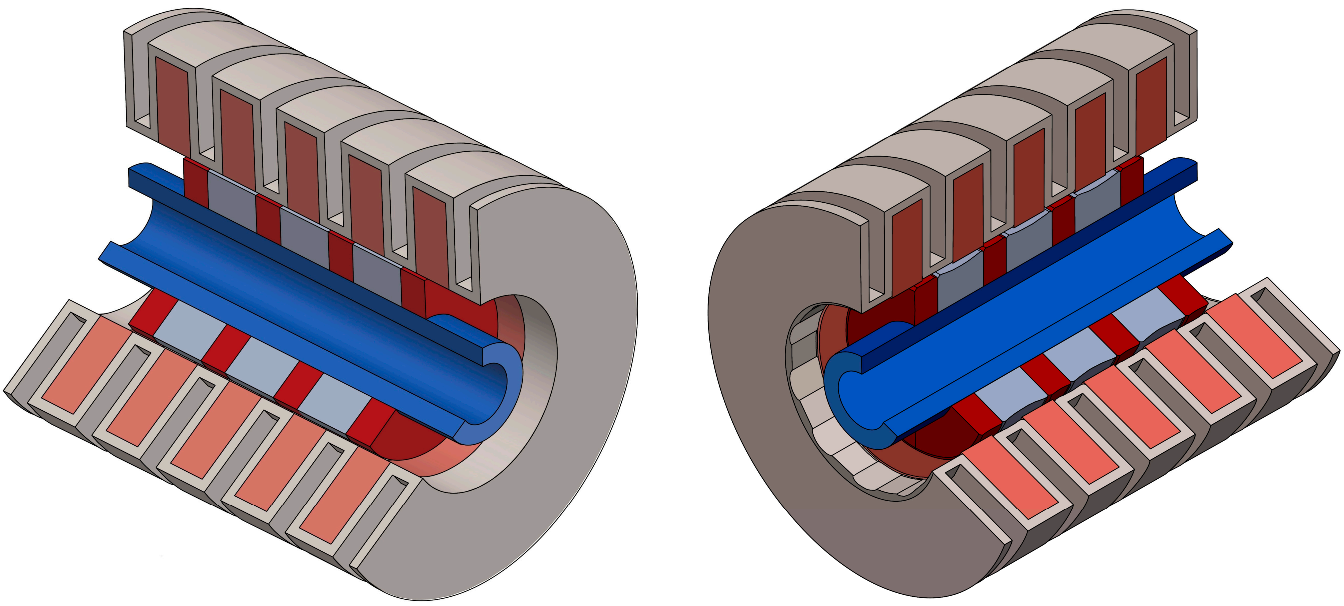

(**a**) (**b**)

Figure 32. Cut-section schematic of the (**a**) original and (**b**) modified model.

Table 2. Chosen values, topology, and parameters for the modified model in comparison with the original model.

Geometrical Alteration	Original Model	Modified Model
Stator tooth edge chamfering—radius of curvature	Nil	1 mm
Magnet tooth edge chamfering—radius of curvature	Nil	0.75 mm
Number of teeth	Six	Six
Axial notching on stator—radius of curvature	Nil	22.5 mm
Axial notching on magnet—radius of curvature	Nil	35 mm
Radial notching on stator—radius of curvature	Nil	9.5 mm
Type of stator notching	Nil	Flat end tooth
Ridging	Nil	Nil
Magnet splitting	One piece	Two pieces

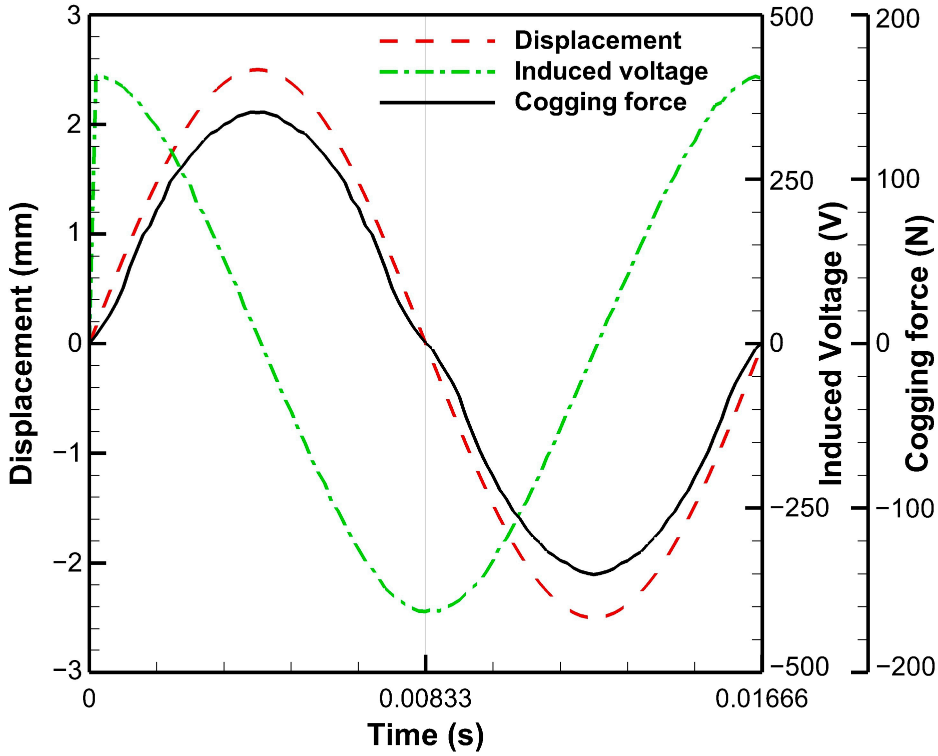

Figure 33. Comparison of induced voltage, cogging force, and displacement of the modified model.

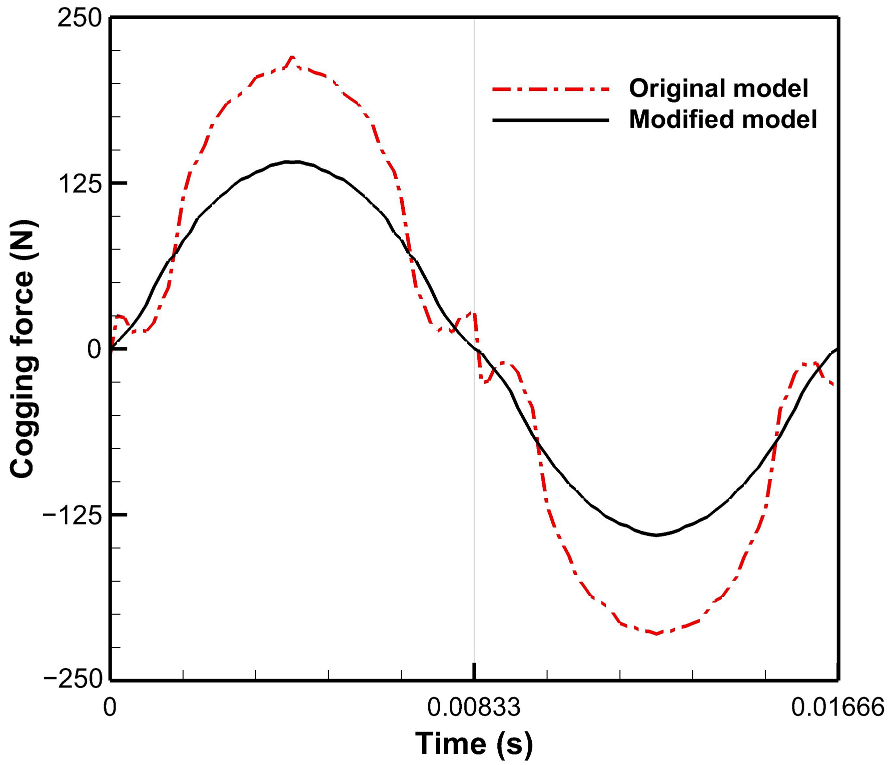

Figure 34. Comparison of original model cogging force with the modified model.

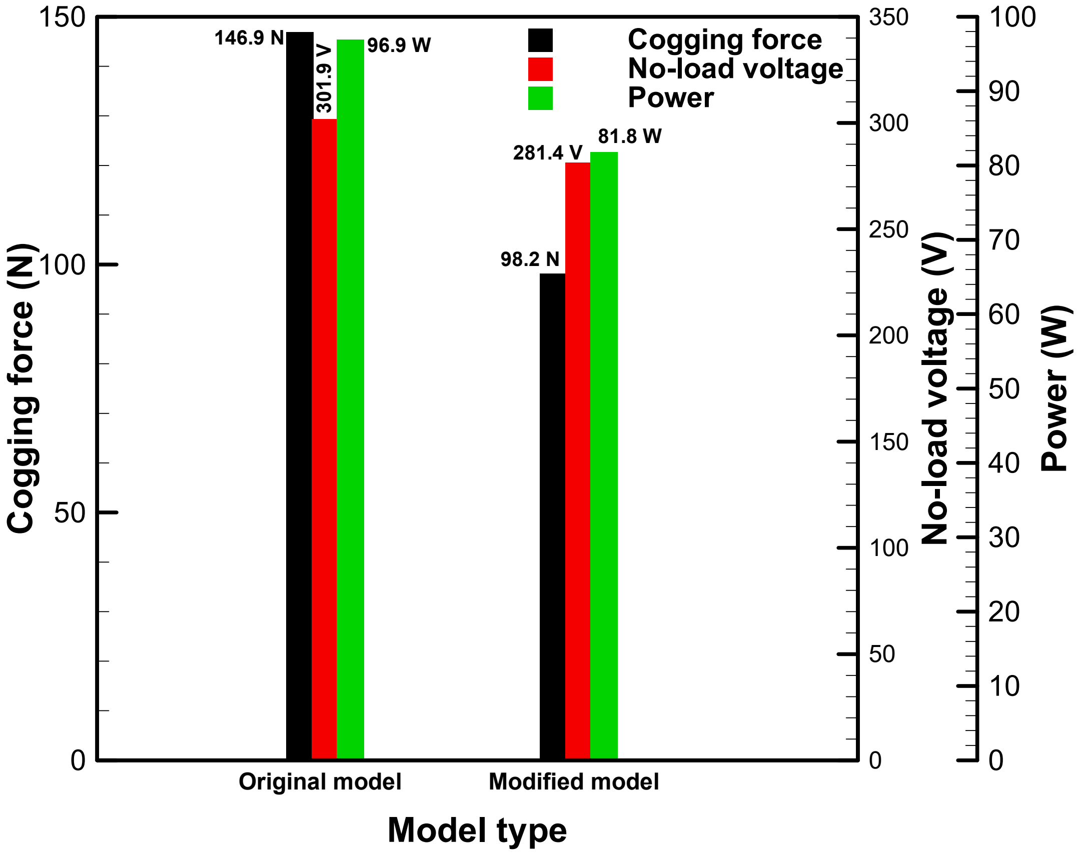

Figure 35. Comparison of performance with the original and the modified model.

6. Conclusions

Cogging force is a parasitic loss and cannot be eliminated. Hence, making design choices inclined towards reducing it will diminish the loss of driving force and increase the power density of permanent magnet linear machines. Considering the aspects of chamfering, notching, tooth elimination, ridging, and magnet splitting will strive for a better PMLA. Geometrical alteration methods such as chamfering, axial notching, and ridging of the stator are novel due to the current lamination process existing in manufacturing technology. This will be an expensive method to construct a stator with such a stacking process. Overcoming these shortcomings and implementing all the geometrical changes discussed to make a modified model can provide a close sinusoidal cogging force profile in line with the displacement of the translator. This avoids unnecessary vibrations on the translator. Overcoming this also improves the operational life of the PMLA. The phase angle difference between the displacement and the cogging force profile is negligible. Implementing the modifications has smoothened the cogging force profile significantly. The modified model produces 15.6% less power than the conventional model, but makes 33.15% less cogging force. This is a significant improvement and meets the original motivation of this study.

Author Contributions: Data curation, S.D.; Formal analysis, C.-H.C.; Investigation, C.-H.C. and S.D.; Methodology, S.D.; Project administration, C.-H.C.; Resources, C.-H.C.; Software, S.D.; Supervision, C.-H.C.; Validation, S.D.; Writing—original draft, S.D.; Writing—review and editing, C.-H.C. All authors have read and agreed to the published version of the manuscript.

Funding: This research received no external funding.

Data Availability Statement: Not applicable.

Acknowledgments: Not applicable.

Conflicts of Interest: The authors declare no conflict of interest.

References

1. Wunderling, N.; Winkelmann, R.; Rockström, J.; Loriani, S.; McKay, D.I.A.; Ritchie, P.D.L.; Sakschewski, B.; Donges, J.F. Global warming overshoots increase risks of climate tipping cascades in a network model. *Nat. Clim. Change* **2022**, *13*, 75–82. [CrossRef]
2. Zhang, S.; Zhou, L.; Zhang, L.; Yang, Y.; Wei, Z.; Zhou, S.; Yang, D.; Yang, X.; Wu, X.; Zhang, Y.; et al. Reconciling disagreement on global river flood changes in a warming climate. *Nat. Clim. Change* **2022**, *12*, 1160–1167. [CrossRef]
3. Santana-Falcón, Y.; Séférian, R. Climate change impacts the vertical structure of marine ecosystem thermal ranges. *Nat. Clim. Change* **2022**, *12*, 935–942. [CrossRef]
4. Holechek, J.L.; Geli, H.M.E.; Sawalhah, M.N.; Valdez, R. A global assessment: Can renewable energy replace fossil fuels by 2050? *Sustainability* **2022**, *14*, 4792. [CrossRef]
5. Gargov, N.P.; Zobaa, A.F.; Pisica, I. Investigation of multi-phase tubular permanent magnet linear generator for wave energy converters. *Electr. Power Compon. Syst.* **2014**, *42*, 124–131. [CrossRef]
6. Durcansky, P.; Nosek, R.; Jandacka, J. Use of Stirling engine for waste heat recovery. *Energies* **2020**, *13*, 4133. [CrossRef]
7. Boldea, I.; Nasar, S.A. *Linear Electric Actuators and Generators*, 4th ed.; Cambridge University Press: Cambridge, UK, 2005; pp. 201–233.
8. Hung, N.B.; Lim, O. A review of free-piston linear engines. *Appl. Energy* **2016**, *178*, 78–97. [CrossRef]
9. Rezaeealam, B. Permanent Magnet Tubular Generator with Quasi-Halbach Array for Free-Piston Generator System. *Int. J. Power Electron. Drive Syst.* **2017**, *8*, 1663. [CrossRef]
10. Cawthorne, W.R.; Famouri, P.; Chen, J.; Clark, N.N.; McDaniel, T.I.; Atkinson, R.J.; Nandkumar, S.; Atkinson, C.M.; Petreanu, S. Development of a linear alternator-engine for hybrid electric vehicle applications. *IEEE Trans. Veh. Technol.* **1999**, *48*, 1797–1802. [CrossRef]
11. Güneş, H. Design and manufacture of tube type nonhollow linear generators for suspension systems of electric and hybrid cars. *Proc. Inst. Mech. Eng. Part E J. Process Mech. Eng.* **2021**, *235*, 1420–1428. [CrossRef]
12. Kim, J.H.; Shin, Y.J.; Chun, Y.D.; Kim, J.H. Design of 100W regenerative vehicle suspension to harvest energy from road surfaces. *Int. J. Precis. Eng. Manuf.* **2018**, *19*, 1089–1096. [CrossRef]
13. Eid, A.M.; Lee, H.W.; Nakaoka, M. Detent Force Reduction of Tubular Linear Generator Using an Axial Stepped Permanent Magnet Structure. *J. Power Electron.* **2006**, *6*, 290–297.
14. Yoshimura, T.; Kim, H.J.; Watada, M.; Torii, S.; Ebihara, D. Analysis of the reduction of detent force in a permanent magnet linear synchronous motor. *IEEE Trans. Magn.* **1995**, *31*, 3728–3730. [CrossRef]
15. Cheng, C.-H.; Dhanasekaran, S. Numerical Analysis and Parametric Study of a 7 kW Tubular Permanent Magnet Linear Alternator. *Sustainability* **2021**, *13*, 7192. [CrossRef]
16. Cheng, C.-H.; Dhanasekaran, S. Design of a Slot-Spaced Permanent Magnet Linear Alternator Based on Numerical Analysis. *Energies* **2022**, *15*, 4523. [CrossRef]
17. Arish, N.; Marignetti, F. Evaluation of Linear Permanent Magnet Vernier Machine Topologies for Wave Energy Converters. *Int. J. Eng.* **2021**, *34*, 403–413.
18. Kumar, P.; Xaxa, L.B.; Srivastava, R.K. Design Modifications for Cogging Force Reduction in Linear Permanent Magnet Machines. In Proceedings of the 2020 IEEE International Conference on Power and Energy (PECon), virtual, 7–8 December 2020.
19. Jang, S.-M.; Lee, S.-H.; Yoon, I.-K. Design criteria for detent force reduction of permanent-magnet linear synchronous motors with Halbach array. *IEEE Trans. Magn.* **2002**, *38*, 3261–3263. [CrossRef]
20. Wang, C.-F.; Shen, J.-X.; Wang, Y.; Wang, L.-L.; Jin, M.-J. A new method for reduction of detent force in permanent magnet flux-switching linear motors. *IEEE Trans. Magn.* **2009**, *45*, 2843–2846. [CrossRef]
21. Seo, S.-W.; Jang, G.-H.; Koo, M.-M.; Choi, J.-Y. Characteristic analysis of the influence of auxiliary teeth and notching on the reduction of the detent force of a permanent magnet linear synchronous machine. *IEEE Trans. Appl. Supercond.* **2018**, *28*, 5203705. [CrossRef]
22. Bucolo, M.; Buscarino, A.; Famoso, C.; Fortuna, L.; Gagliano, S. Imperfections in integrated devices allow the emergence of unexpected strange attractors in electronic circuits. *IEEE Access* **2021**, *9*, 29573–29583. [CrossRef]